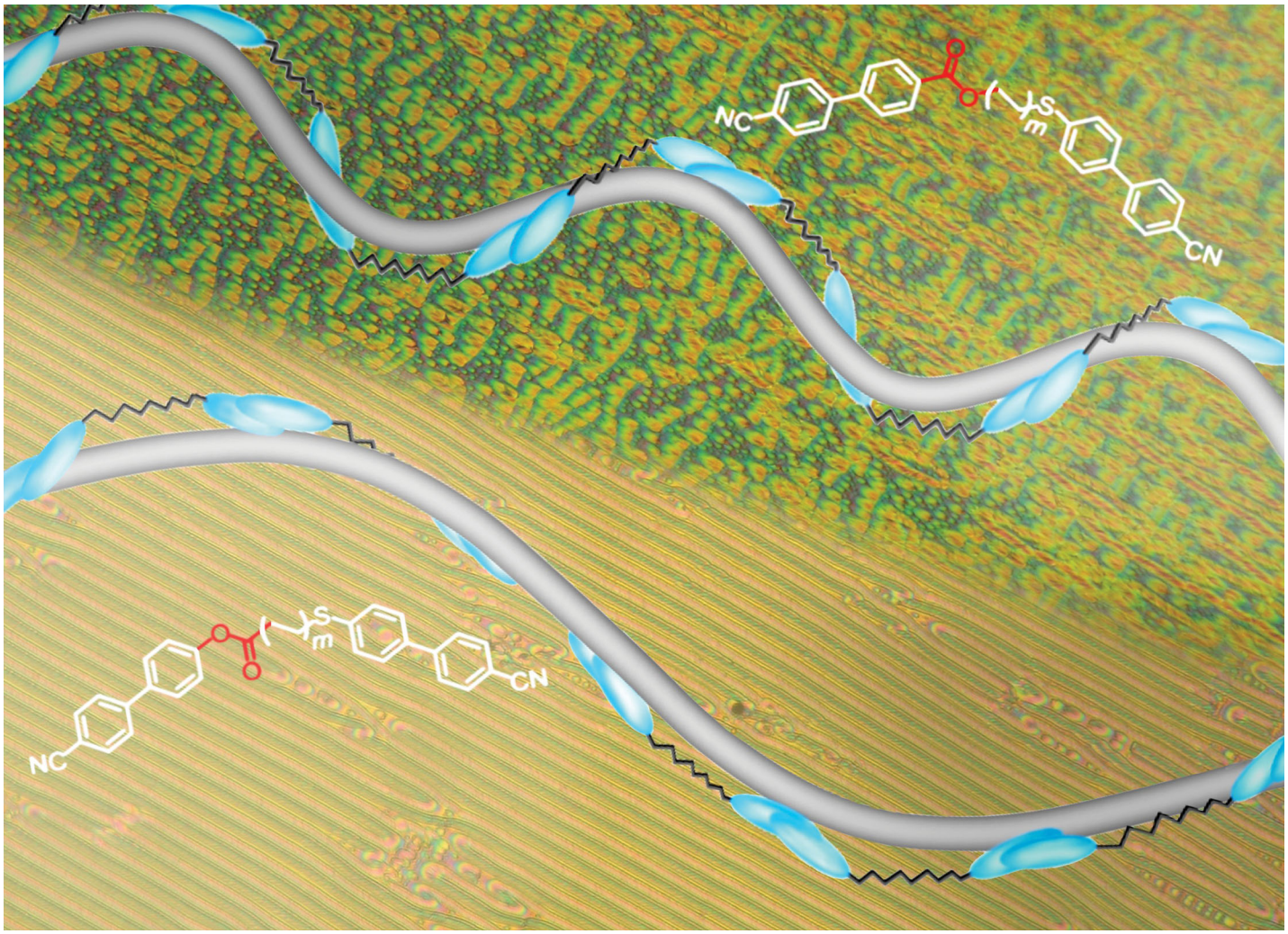

Showcasing research from Assistant Professor Arakawa's group, Department of Applied Chemistry and Life Science, Toyohashi University of Technology, Toyohashi, Japan.

Distinct twist-bend nematic phase behaviors associated with the ester-linkage direction of thioether-linked liquid crystal dimers

We demonstrated the distinct helical twist-bend nematic phase behaviors associated with the ester-bond direction in two homologous series of sulfur-linked cyanobiphenyl liquid-crystal (LC) dimers (CBCOO*n*SCB and CBOCO*n*SCB) with different molecular bend angles. We developed both homologous series and found that the helical pitches for CBOCO*n*SCB were approximately double than those of CBCOO*n*SCB using tender resonant X-ray scattering at the sulfur K-edge. The pitches of CBOCO*n*SCB and CBCOO*n*SCB were longer and shorter than those of the usual LC dimers, respectively. The molecular bend (or biaxiality) of LC dimers strongly impacts the helical pitch.

As featured in:

See Yuki Arakawa *et al.*, *Mater. Adv.*, 2021, **2**, 261.

ROYAL SOCIETY OF CHEMISTRY

rsc.li/materials-advances

Registered charity number: 207890

Materials Advances

ROYAL SOCIETY OF CHEMISTRY

PAPER

View Article Online
View Journal | View Issue

Cite this: *Mater. Adv.*, 2021, **2**, 261

Distinct twist-bend nematic phase behaviors associated with the ester-linkage direction of thioether-linked liquid crystal dimers†

Yuki Arakawa, *[a] Kenta Komatsu,[a] Jun Feng,[b] Chenhui Zhu [b] and Hideto Tsuji [a]

The twist-bend nematic phase (N_{TB}) is a new spontaneous symmetry-breaking phenomenon observed in fluidic liquid crystal (LC) phases, which possesses a heliconical structure with a pitch ranging from several to tens of nanometers. Herein we demonstrate the distinct nano-to-macroscopic N_{TB} phase behaviors associated with the ester-bond direction in two homologous series of sulfur-containing cyanobiphenyl-based LC dimers, *viz.* CBCOO*n*SCB and CBOCO*n*SCB (*n* = 2, 4, 6, 8, and 10). Both the series (excluding *n* = 2) formed N_{TB} phases in which the homologues (*n* = 4 and 6) exhibited the N_{TB} phases across a broad temperature range, which were observed to be stable even at room temperature and eventually formed N_{TB} glasses. We found that both homologues (*n* = 4 and 6) displayed distinct phase-transition properties and optical textures with respect to the N_{TB} phases. By performing tender resonant X-ray scattering measurements at the sulfur K-edge, we discovered their distinctly different nanoscopic helical pitch lengths. Within a similar shifted temperature, the pitches for CBOCO*n*SCB showed strong temperature dependence and were approximately double those of CBCOO*n*SCB, which exhibited significantly weaker temperature dependence. Compared to those of the representative twist-bend nematogenic dimers, the pitches of CBOCO*n*SCB and CBCOO*n*SCB are longer and shorter, respectively. It is assumed that the molecular bend (or the molecular biaxiality) of LC dimers strongly influences the precession angle of the heliconical helix, and hence the resulting pitch. These findings provide new insights into the molecular designs to modulate the nanoscale helical pitches of the N_{TB} phases.

Received 29th September 2020,
Accepted 7th November 2020

DOI: 10.1039/d0ma00746c

rsc.li/materials-advances

Introduction

Liquid crystals (LCs) are involved in several spontaneous symmetry-breaking phenomena associated with chirality and helices, which have been the subject of great interest in the field of molecular sciences.[1–10] At present, the twist-bend nematic (N_{TB}) phase, a new helical LC phase, is a hot research topic in the field of LCs. Although the N_{TB} phase was theoretically proposed[11,12] and simulated in earlier works,[13] it has only recently been experimentally demonstrated with a bent achiral dimer.[14] The N_{TB} phase is believed to originate from the twist and bend deformations of bent molecules, resulting in a heliconically arranged director periodicity, wherein the local director tilts against the helical axis. Due to this phenomenon, right- and left-handed helical nanostructures and their associated degenerate domains are observed to spontaneously form, even from achiral molecules. On the other hand, another model, named the polar-twisted nematic (N_{PT}) phase, for the heliconical mesophase identified as the N_{TB} phase was proposed, which is under debate.[15–17] Macroscopic chirality of the N_{TB} phase was verified using circular dichroism spectroscopy.[18] Several techniques, including electro-optical measurements,[19] freeze-fracture transmission electron microscopy,[20,21] and resonant soft, hard, and tender X-ray scattering measurements,[22–27] suggest that the helical pitch of an N_{TB} phase formed by several molecules is ~10 nm, which is significantly shorter than the pitch of a typical chiral N phase or cholesteric phase exhibiting a helicoidal helix (generally hundreds of nanometers). Materials that exhibit the N_{TB} phase have been employed for various LC applications, such as wavelength-tunable selective light reflection[28–31] and optical memory[32] devices, LC physical gels,[33] photo-switchable viscoelastic bodies,[34] and photoalignment technology.[35]

[a] *Department of Applied Chemistry and Life Science, Graduate School of Engineering, Toyohashi University of Technology, Toyohashi, 441-8580, Japan. E-mail: arakawa@tut.jp*
[b] *Advanced Light Source, Lawrence Berkeley National Laboratory, Berkeley, CA, 94720, USA*

† Electronic supplementary information (ESI) available. See DOI: 10.1039/d0ma00746c

To date, a number of bent LC dimers composed of two mesogenic structures connected with an odd-numbered oligomethylene spacer have been shown to exhibit the N_{TB} phase.[36–57] In addition, several LC oligomers (*e.g.*, trimers,[53,58–63] tetramers,[58,59,64] a hexamer,[65] and other types of oligomers[66–69]), polymers,[70] and bent-core molecules[71,72] have also been identified as twist-bend nematogens. It should be noted here that the bent molecular geometry is key to designing twist-bend nematogens. The angle of the molecular bend and the stability of the N_{TB} phase are highly dependent on the bonds linking the two rigid mesogenic arms and the flexible oligomethylene spacer; *e.g.*, methylene-linked cyanobiphenyl (CB)-based CB*n*CB dimers (representative twist-bend nematogens)[14,36,37] and ether-linked CBO*n*OCB dimers (conventional nematogens).[73] Mandle *et al.* comprehensively studied the relationship between the bend angle of several CB dimers with different linkages and their N_{TB} formation using both experimental and quantum calculation approaches.[45,54] In addition, the influence of various combinations of chalcogens and other linkages on the N_{TB} phase incidence and stability has been studied.[52,53] We previously reported[53] a number of systematically designed thioether-linked LC dimers to ascertain the molecular design necessary to form the N_{TB} phase; unsymmetrical ester- and thioether-linked CB-based dimers with a butylene spacer, *viz.* CBCOO4SCB and CBOCO4SCB (Fig. 1), formed N_{TB} phases when supercooled to room temperature to be a N_{TB} glass (N_{TB}G). The latter displayed behaviors typically observed in twist-bend nematogens, including a second-order-like N–N_{TB} transition and clear blocky, focal conic, and striped textures. Whereas the former CBCOO4SCB exhibited unusual behaviors such as a first-order-like N–N_{TB} transition and ambiguous striped optical textures that were extremely thin. The origin of such differences between the dimers is yet to be determined. One possibility is that these phenomena may be a consequence of the distinct helical structures present at the nanoscale due to oppositely directed ester-linkages. Evaluation of the helical pitches of a homologous series of dimers using tender resonant X-ray scattering (TReXS) at the sulfur K-edge can be one of the most helpful techniques to understand such nano-to-macroscopic structural associations.[24–27]

This is the first report of the synthesis, detailed phase-transition behaviors, and distinct nano-to-macroscopic N_{TB} phase behaviors associated with different heliconical nanostructure modes of two homologous series of sulfur-containing LC dimers with oppositely directed ester-linkages. Unsymmetrical ester- and thioether-linked CB-based dimer homologues were synthesized, *viz.* CBCOO*n*SCB and CBOCO*n*SCB (n = 2–10, even numbers only), which contain oppositely directed esters (*i.e.*, –C═OO– and –OC═O–, respectively). The number of carbon atoms in the oligomethylene spacers (n) were selected such that the total number of atoms in the linkage and the spacer along the chain is an odd number, thereby giving an overall bent molecular geometry. We evaluated the phase transitions and mesomorphism of the dimers using polarized optical microscopy (POM), differential scanning calorimetry (DSC), and conventional X-ray diffractometry (XRD), and analyzed the heliconical structures using TReXS at the sulfur K-edge.

Results and discussion

The synthetic procedures and characterization of the homologous series of CBCOO*n*SCB and CBOCO*n*SCB are described in the ESI.† Their phase sequences, phase-transition temperatures at crystallization (T_{Cr}), glass transition (T_g), N–N_{TB} phase transition (T_{NNTB}), isotropic (I)–N phase transition (T_{IN}), entropy changes (ΔS) scaled by the gas constant (R) at the I–N and N–N_{TB} phase transitions ($\Delta S_{IN}/R$ and $\Delta S_{NNTB}/R$, respectively), and T_{NNTB}/T_{IN} at a cooling rate of 10 °C min^{-1} are summarized in Table 1. The phase-transition data obtained during the first heating are listed in Tables S1 and S2 (see ESI†).

In terms of the phase-transition behavior of the CBCOO*n*SCB series, the dimers with n = 4, 6, 8, and 10 exhibited a monotropic N_{TB} phase below the N phase, whereas the shortest CBCOO2SCB dimer exhibited only a monotropic N phase. The monotropic N phase of CBCOO2SCB appeared at 83 °C and was partially supercooled to room temperature upon cooling. This N phase could only be observed using POM due to crystallization of the dimer (Fig. S1 and S9, ESI†). CBCOO6SCB and CBCOO8SCB displayed transitions to the N_{TB} phase from the corresponding N phase at 75 and 85 °C, respectively. Notably, CBCOO6SCB exhibited the N_{TB} phase across a broad temperature range, which was supercooled to room temperature and ultimately underwent vitrification to form a N_{TB}G, similar to CBCOO4SCB.[53] The DSC curves of CBCOO6SCB are shown in Fig. 2(a). The N–N_{TB} phase-transition peak was identified as a first-order-like transition with a $\Delta S_{NNTB}/R$ value of 0.54, which differs from the second-order-like transition behavior typically observed for twist-bend nematogens. The N_{TB} phase of CBCOO8SCB crystallized at 76 °C and the dimer bearing the longest spacer (*i.e.*, CBCOO10SCB) also exhibited the N_{TB} phase, but underwent crystallization at approximately 90 °C, as can be seen from the DSC curves (Fig. S11 and S12, ESI†); the N_{TB} phases could be

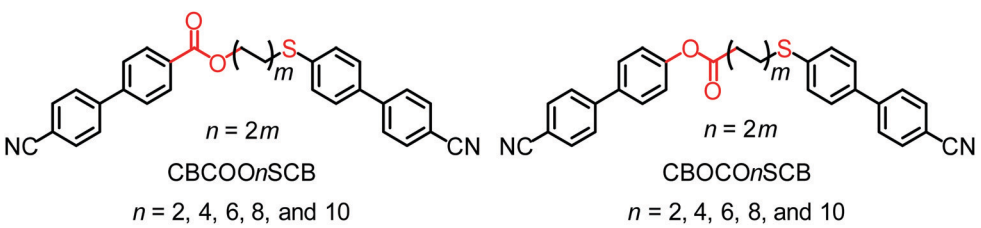

Fig. 1 Molecular structures of CBCOO*n*SCB (n = 2, 4, 6, 8, and 10) and CBOCO*n*SCB (n = 2, 4, 6, 8, and 10), where n = 2m.

Table 1 Phase sequences, transition temperatures (°C), and entropy changes scaled by the gas constant ($\Delta S/R$) of CBCOO*n*SCB and CBOCO*n*SCB upon cooling

n (CBCOO*n*SCB)		T_{Cr} (°C)	$\Delta S_{Cr}/R$		T_{NNTB} (°C)	$\Delta S_{NNTB}/R$		T_{IN} (°C)	$\Delta S_{IN}/R$		T_{NNTB}/T_{IN}
2	Cr	129.0	11.8	—	—	—	—	83[a]	—	I	—
4	G	20.7	—	N_{TB}	52.3	0.18	N	68.7	0.02	I	0.95
6	G	22.3	—	N_{TB}	75.4	0.54	N	87.1	0.09	I	0.97
8	Cr	75.8	12.6	N_{TB}	85[a]	—	N	99.0	0.30	I	0.96
10	Cr	90.3	12.1	N_{TB}	87[a]	—	N	104.9	0.40	I	0.95
n (CBOCO*n*SCB)											
2	Cr	131.0	10.1	—	—	—	N	134[a]	—	I	—
4	G	17.5	—	N_{TB}	82.3	—	N	150.0	0.46	I	0.84
6	G	14.3	—	N_{TB}	94.9	—	N	149.0	0.57	I	0.87
8	Cr	78.7	10.7	N_{TB}	93[a]	—	N	145.4	0.84	I	0.87
10	Cr	97.4	10.9	N_{TB}	91[a]	—	N	140.6	1.11	I	0.88

[a] Determined by POM.

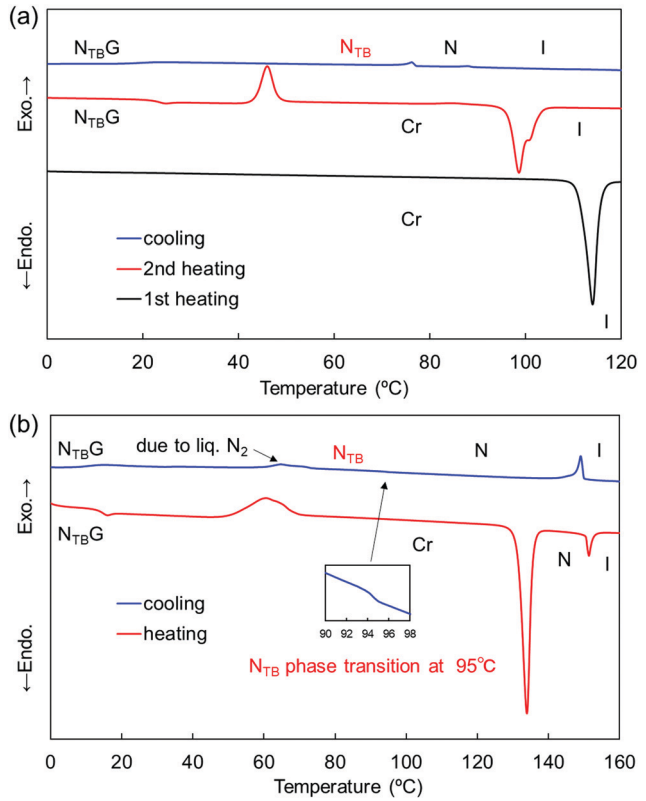

Fig. 2 DSC curves of (a) CBCOO6SCB and (b) CBOCO6SCB recorded at a rate of 10 °C min^{-1}.

observed only in small supercooled N domains using POM (Fig. S3, S5, S7 and S8, ESI†).

Regarding the phase-transition behavior of the CBOCO*n*SCB series, dimers with n = 4, 6, 8, and 10 formed a monotropic N_{TB} phase below the N phase temperature. Like CBCOO2SCB, the dimer with the shortest spacer (CBOCO2SCB) only formed the monotropic N phase. The N phase of CBOCO2SCB was very narrow, which could be observed by POM but was not detected by DSC due to crystallization during cooling (Fig. S6 and S13, ESI†). As shown in Fig. 2(b), CBOCO6SCB exhibited a remarkably stable N_{TB} phase when supercooled to room temperature, with vitrification taking place at 14 °C to form the $N_{TB}G$ phase; this behavior is similar to that of CBOCO4SCB.[53] Furthermore, the N–N_{TB} phase transition at 94.9 °C is similar to the second-order-like phase-transition typically observed for the majority of twist-bend nematogens. CBOCO8SCB exhibited the N_{TB} phase at temperatures ranging from 93 to 79 °C, below which it underwent crystallization. The N–N_{TB} phase transition at 85 °C could not be detected by DSC due to crystallization (Fig. S16, ESI†). Moreover, the N_{TB} phase was observed only in the supercooled N domains of CBOCO10SCB; hence, no N–N_{TB} transition peak could be detected *via* DSC (Fig. S8 and S17, ESI†). Unlike CBCOO*n*SCB, which exhibited monotropic mesophases, CBOCO*n*SCB with n = 4, 6, 8, and 10 gave rise to enantiotropic N phases. In addition, the abovementioned observations indicate that mid-length spacers (n = 4 and 6) of both homologous series enhanced the N_{TB} phase ranges, which ultimately resulted in the formation of a room-temperature N_{TB} phase or $N_{TB}G$ phase.

The T_{IN}, T_{NNTB}, and $\Delta S_{IN}/R$ values as a function of n for CBCOO*n*SCB and CBOCO*n*SCB (n = 4, 6, 8, and 10) are displayed in Fig. 3. The phase-transition temperatures are higher for CBOCO*n*SCB than for CBCOO*n*SCB, except T_g. This difference can be attributed primarily to their different geometries according to the all-*trans* model of spacer chains; in other words, their molecular biaxiality and shape anisotropy. The inter-arm bend angle (α) between the *para*-axes of the two mesogenic arms of CBCOO4SCB (α = 105°) is significantly smaller than that of CBOCO4SCB (α = 127°).[53] This difference is caused by the opposed ester-bond directions or the different positions of carbonyl (C═O) and –O–C– bonds in the esters. Notably, the T_{IN} values of CBCOO*n*SCB were found to strongly depend on n, whereas those of CBOCO*n*SCB were only slightly affected by n. The T_{NNTB} values of CBCOO*n*SCB sharply decreased with a decrease in n, while the corresponding values of CBOCO*n*SCB did not. It is worth noting that the $\Delta S_{IN}/R$ values are significantly smaller for CBCOO*n*SCB than for CBOCO*n*SCB. The abovementioned trends may be associated with the more bent geometry of CBCOO*n*SCB with the smaller bend angle or the more anisotropic geometry of CBOCO*n*SCB.[48] The $\Delta S_{IN}/R$ values of both homologous series were found to gradually decrease with decreasing n, which can be ascribed to the molecular structural biaxiality that is enhanced by

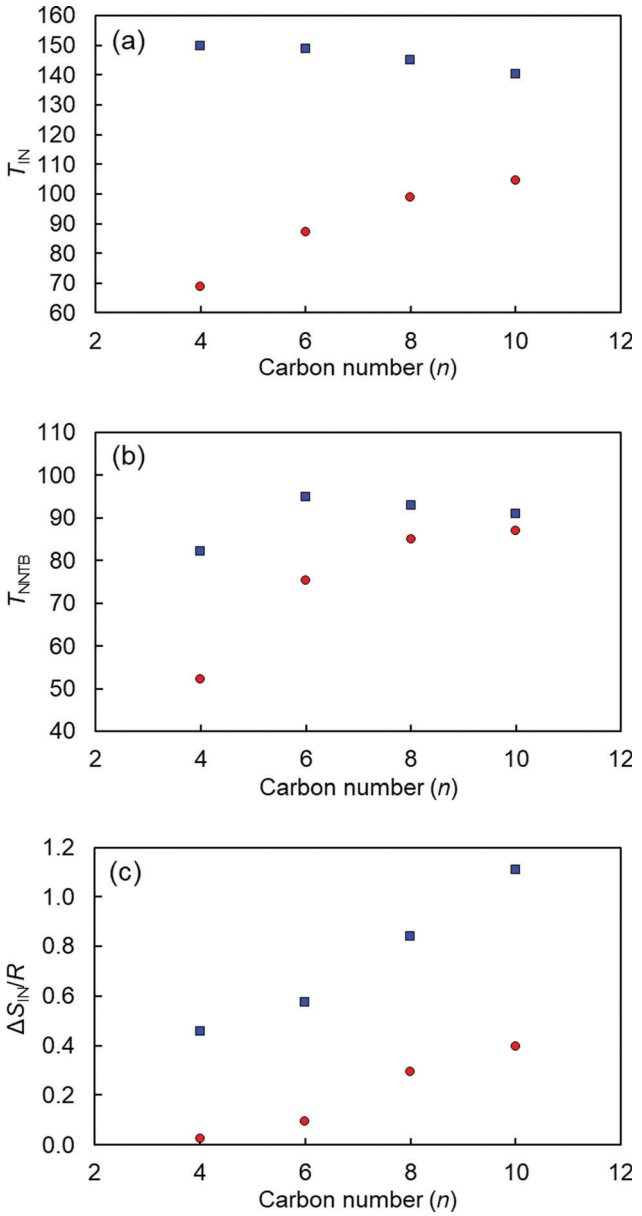

Fig. 3 (a) T_{IN}, (b) T_{NNTB}, and (c) $\Delta S_{IN}/R$ values as a function of n for CBCOOnSCB with n = 4, 6, 8, and 10 (red circles) and CBOCOnSCB with n = 4, 6, 8, and 10 (blue squares).

decreasing the spacer length, thereby reducing molecular anisotropy. In addition, the reduced temperature, T_{NNTB}/T_{IN}, values for CBOCOnSCB ($\sim$0.86) were smaller than those for CBCOOnSCB ($\sim$0.96), and these values remained nearly constant within each homologous series. This reflects that the N–N_{TB} phase of CBOCOnSCB originates from the supercooled N phases, which undergo a greater degree of supercooling than those of CBCOOnSCB. These trends can also be reasonably associated with their molecular geometry or anisotropy. More bent molecules can effectively form the N_{TB} phase, whereas more linear molecules typically favor formation of the conventional N phase. Hence, appearance of the N_{TB} phase for CBOCOnSCB is naturally induced from the more supercooled N phase, resulting in lower T_{NNTB}/T_{IN} values.[56]

Using POM, we observed different optical textural behaviors in the N_{TB} phases for each homologous series when n = 4 and 6. In non-treated glass cells, CBCOOnSCB (n = 4 and 6) exhibited focal conic textures (Fig. S2, ESI†),[53] which are typical of the N_{TB} phase. In addition, they displayed textures characterized by an elastic behavior (Fig. S2, ESI†); these textures could be recovered even when expansion took place through pressing and shearing. In our previous report,[53] we noted that CBCOO4SCB exhibited unusual striped texture with an obscure thinner-striped texture as shown in Fig. 4(a) using POM with a uniaxially rubbed planar cell. In this study, we conducted further POM analyses of CBOCO4SCB, CBOCO6SCB, CBCOO6SCB, and CBCOO8SCB using 5 μm-thick uniaxially rubbed polyimide-surface-treated planar alignment cells. We found that CBOCO4SCB exhibited the usual optical texture of the N_{TB} phase with clear stripes [Fig. 4(c)], which is distinct from the obscure thin stripes found in CBCOO4SCB [Fig. 4(a)]. The two dimers with n = 6 also displayed clearly different optical texture behaviors: CBCOO6SCB exhibited a distinct thinner-striped texture [Fig. 4(b)]; however, CBOCO6SCB displayed a more typical striped texture [Fig. 4(d)]. These were similar to the different texture behaviors of CBCOO4SCB and CBOCO4SCB. Meanwhile, CBCOO8SCB exhibited a conventional striped texture that was similar to those of the typical twist-bend nematogens and the oppositely directed esters, CBOCO4SCB and CBOCO6SCB (Fig. S4, ESI†). It seems that the unusual textures with thinner stripes observed for CBCOOnSCB were changed to the typical ones with increasing length of the central spacer. In addition to the properties associated with the first and second order phase-transitions of the N_{TB} phases of CBCOOnSCB and CBOCOnSCB (n = 4 and 6), respectively, the observed textural patterns inspired us to study the helical structures of the N_{TB} phases by means of comprehensive X-ray techniques, since previous studies suggested the presence of heliconical structures[19–27] and pseudo-layer nature in the N_{TB} phase.[74,75]

To analyze the structures of the observed mesophases, we firstly conducted conventional XRD measurements for both homologous series with n = 4 and 6 (Fig. S18–S21, ESI†). In both the N and N_{TB} phases, broadened diffraction peaks were observed in the small- and wide-angle regions. These results suggest that there is no apparent positional order along the long molecular axis, and liquid-like correlations exist among lateral molecules, thereby indicating the nature of the N phase. In addition, the small-angle diffraction pattern corresponds to pseudo-layered structures that originate from the smectic (Sm)-like or cybotactic molecular clusters in the N and N_{TB} phases. The pseudo-layer lengths in the N_{TB} phase were estimated to be similar: 1.15 nm (2θ = 7.6°) for CBCOO4SCB, 1.27 nm (2θ = 6.9°) for CBCOO6SCB, and 1.32 nm (2θ = 6.7°) for CBOCO6SCB in each N phase. The intensity of the small-angle diffraction was weaker in the N_{TB} phase than in the N phase, and the 2θ values (or the pseudo-layer lengths) were temperature-independent over the entire N_{TB} phase range, which is typical of N_{TB} phases. In the case of CBOCO4SCB, the small-angle diffraction could

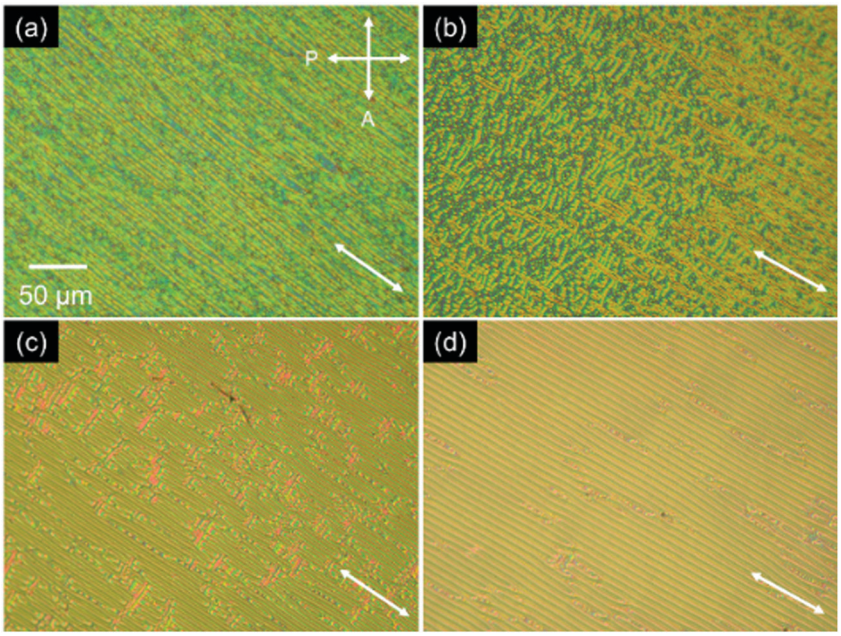

Fig. 4 POM images of the N_{TB} phases of (a) CBCOO4SCB, (b) CBCOO6SCB, (c) CBOCO4SCB, and (d) CBOCO6SCB in a uniaxially rubbed cell with planar alignment. The POM image in panel (a) is reproduced from ref. 53 with permission from Elsevier.

only be detected in the N phase, disappearing after transition to the N_{TB} phase (Fig. S20, ESI†).

We performed TReXS measurements at the sulfur K-edge to determine the helical pitch in the N_{TB} phases of CBCOO*n*SCB and CBOCO*n*SCB (n = 4 and 6). TReXS at the sulfur K-edge enables the detection of resonant scattering that corresponds to the helical pitch in the N_{TB} phase, owing to the periodically distributed bond direction (rather than the conventional electron density modulation) in heliconical structures.[24–27] The two-dimensional (2D) and one-dimensional (1D) resonant X-ray scattering patterns obtained from the helical pitch periodicity in the N_{TB} phase of CBCOO4SCB are shown as representative images in Fig. 5. These scattering patterns appeared at temperatures below the N phase upon cooling and disappeared upon re-entering the N phase upon reheating. The 2D scattering images of the other dimers and the corresponding 1D patterns are shown in Fig. S22–S27 (ESI†). Fig. 6(a) shows the temperature dependence of the helical pitch in the N_{TB} phase for both the homologous series (n = 4 and 6) as a function of the shifted temperature ($\Delta T = T_{NNTB} - T$). The helical pitch lengths (p_h) were calculated from the wavenumber $q = 2\pi/p_h$. Upon decreasing the temperature, the p_h values decreased from 8.1 to 6.8 nm for CBCOO4SCB and from 9.3 to 7.4 nm for CBCOO6SCB, while those of CBOCO4SCB and CBOCO6SCB decreased from 20.3 to 11.9 nm and from 24.4 to 13.8 nm, respectively. Compared with those of CBOCO4SCB and CBOCO6SCB, the helical pitches of CBCOO4SCB and CBCOO6SCB were not only significantly shorter but also less temperature-dependent. The helical pitch lengths of

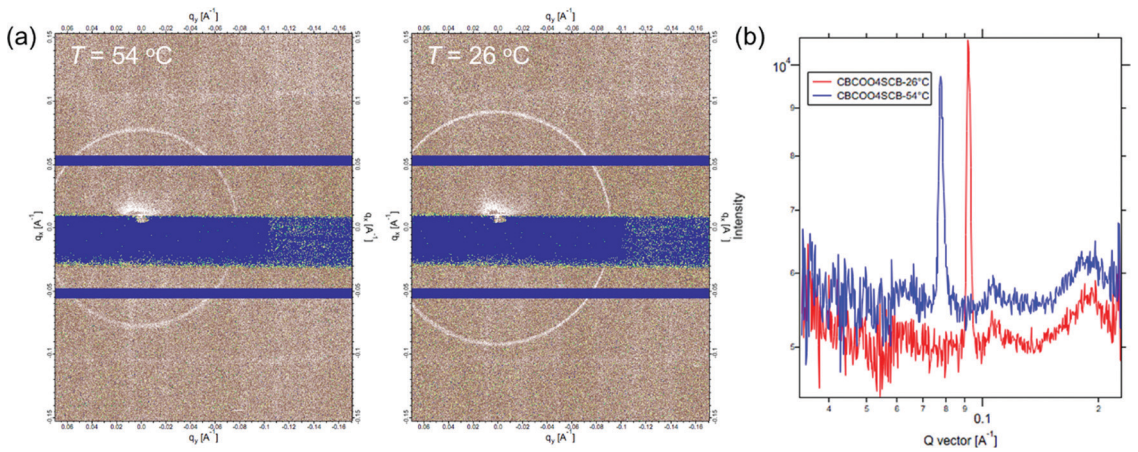

Fig. 5 (a) Typical 2D-scattered patterns and (b) the corresponding 1D patterns in the N_{TB} phase of CBCOO4SCB. Note the horizontal blue streaks in (a) are areas with no data, either due to gaps between detector modules or the beam stop used to block the direct X-ray beam.

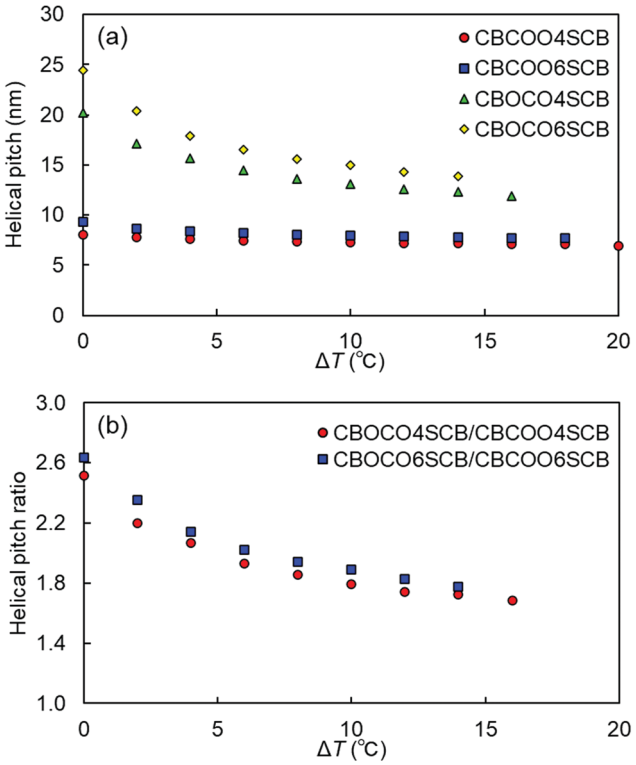

Fig. 6 (a) Helical pitches of CBCOO4SCB, CBCOO6SCB, CBOCO4SCB, and CBOCO6SCB, and (b) helical pitch ratios of CBOCO4SCB/CBCOO4SCB and CBOCO6SCB/CBCOO6SCB as a function of the shifted temperature ($\Delta T = T_{NNTB} - T$).

CBOCO4SCB and CBOCO6SCB decreased upon lowering the temperature, as is typical for N_{TB} phases; this temperature dependence may be attributed to the lower number of twisted molecular conformations (or an increase in straightened conformers)[76] and fluctuations in the unwinding process related to helical ordering at high temperatures, which relate to decreased precession of the molecules in the helices at high temperatures. However, the helical pitch lengths of CBCOO4SCB and CBCOO6SCB do not vary significantly at different temperatures. Furthermore, it is noteworthy that the p_h ratios of p_h(CBOCO4SCB)/p_h(CBCOO4SCB) and p_h(CBOCO6SCB)/p_h(CBCOO6SCB) are close to 2, *i.e.*, the helical pitch lengths of CBOCO*n*SCB (n = 4 and 6) were twice those of CBCOO*n*SCB (n = 4 and 6), as shown in Fig. 6(b). Density functional theory (DFT) calculations using Gaussian 16 at the B3LYP 26/6-31G(d) level of theory show that the difference in the overall molecular lengths of CBCOO4SCB (2.56 nm) and CBOCO4SCB (2.78 nm) is small; therefore, the considerable difference in their helical pitches cannot be qualitatively accounted for by the molecular lengths, which will be discussed later.

The helical pitch length is associated with the tilt angle from the helical axis (θ), molecular length (L), and molecular number per turn (n_m) (see Fig. 7); $p_h = n_m L \cos\theta$, and hence n_m can be estimated by calculating the value of $2\pi/qL\cos\theta$. With decreasing temperature, the θ values for LC dimers typically increase by 10 to 35°.[23,26,77–81] Nevertheless, it is realistically assumed that θ does not significantly influence the n_m values within the heliconical region. In the low temperature region of the N_{TB} phase, the n_m values were estimated as n_m = 3–4 for CBCOO4SCB and CBCOO6SCB and n_m = 5–6 for CBOCO4SCB and CBOCO6SCB within a similar ΔT region.

Next, the helical models of the dimers were considered based on XRD and TReXS. The azimuthal precession (φ) per

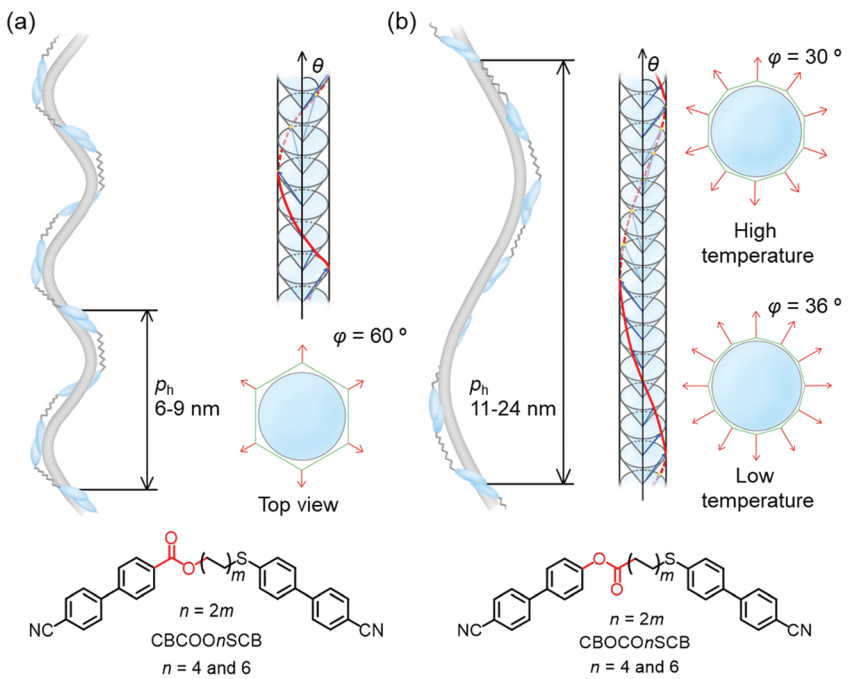

Fig. 7 Plausible heliconical helix models in the N_{TB} phases of (a) CBCOO4SCB and CBCOO6SCB, and of (b) CBOCO4SCB and CBOCO6SCB.

pseudo-layer was estimated from the following equation: $\Delta\varphi$ = 360° × (pseudo-layer length on XRD)/(p_h on TReXS); this can be used to elucidate the heliconical models by utilizing the polygon models.[61] The φ values were estimated to be ~60° in the N_{TB} phase of CBCOO*n*SCB (n = 4 and 6). These φ values indicate a hexagonal model separated by pseudo-layers for the N_{TB} phase of CBCOO*n*SCB (n = 4 and 6). On the other hand, the φ values of CBOCO*n*SCB (n = 4 and 6) essentially became smaller (approximately 30–40°) within the tested temperatures or led to the formation of larger polygonal structures such as a decagon due to their abnormally long helical pitches. The φ values of CBOCO4SCB were estimated using the pseudo-layer length in the N phase since the pseudo-layer peak almost disappeared below the N_{TB} phase.

Using the values of n_m and $\Delta\varphi$, we constructed two heliconical models in the N_{TB} phases of CBCOO*n*SCB and CBOCO*n*SCB (n = 4 and 6). Fig. 7(a) and (b) illustrate plausible heliconical models with n_m = 3–4 and $\Delta\varphi$ = 60° for a hexagon model of CBCOO*n*SCB (n = 4 and 6) and with n_m = 6–7 for CBOCO*n*SCB (n = 4 and 6), respectively. Considering the strong temperature dependence of the helical pitches in the latter, it is assumed that the bent conformation and the stacking extent of the rigid CB arms among the dimers may also be influenced by temperature, changing the precession angles.

As described in the Introduction, the p_h values of the N_{TB} phase are ~10 nm,[19–27] corresponding to several dimers. For example, the p_h of CB7CB, which is a representative twist-bend nematogen structurally analogous to CBCOO*n*SCB and CBOCO*n*SCB dimers, has been found to vary between 8 and 10 nm depending on the temperature.[22] However, the p_h values of both CBCOO*n*SCB (n = 4 and 6) were found to be somewhat smaller than those of CB7CB, while those of CBOCO*n*SCB (n = 4 and 6) were larger. That is, the oppositely directed esters caused unique and distinct helical structural modes in the N_{TB} phases of these dimers which differ from those of the typical dimer. CBCOO*n*SCB (α = 105°) can be bent to a higher extent than CBOCO*n*SCB (α = 127°), which are ascribed to the opposed ester-bond directions or the different positions of carbonyl (C═O) and –O–C– bonds in the two type esters.[53] In addition, the linkage point between CB and –COO– of CBCOO*n*SCB is more rigid than that between CB and OCO CBOCO*n*SCB. The rotational barrier of the –C(Ar)–C═ bond in CBCOO*n*SCB is higher than that of the –C(Ar)–O– bond in CBOCO*n*SCB.[82–85] Thus, the increased bending and more rigid structure of CBCOO*n*SCB should result in shorter helical pitches and a weaker temperature dependence, as compared with those of CBOCO*n*SCB and the other reported twist-bend nematogenic dimers. This can be associated with the first-order-like N–N_{TB} transition peak that corresponds to the changes in the phase structure.

The main factor responsible for the longer helical pitch of CBOCO*n*SCB (*i.e.*, approximately 10–25 nm) as compared to that of CB7CB (8–10 nm) is likely to be the molecular bend (or the molecular biaxiality) and the resulting precession angles of the helices. The molecular bend angle of CB*n*CB is estimated as 111° based on its all-*trans* model,[45] leading to a more bent geometry for CB*n*CB than for CBOCO*n*SCB (127°).[53]

On the other hand, the p_h values of both ester homologous series were marginally shorter in homologues with n = 4 than those with n = 6, due to the different lengths of flexible spacer chains. As illustrated in Fig. 6, the temperature dependence of the p_h values remained essentially unchanged for both the systems.

Finally, we estimated the correlation lengths of the helices and the number of the helical stacks in the N_{TB} phases of CBCOO*n*SCB and CBOCO*n*SCB (n = 4 and 6). Using the full width at half maximum (FWHM) of the Lorentzian fitting (FWHM = 2/ξ, where ξ is the Lorentzian length) applied to the TReXS data, the Scherrer equation (τ = 2π/FWHM; wherein the shape factor is set to unity) can be used to estimate the longitudinal heliconical correlation or domain size.[23] In addition, the number of helical stacks was estimated by calculating τ/p_h. The longitudinal correlation lengths and helical stacks are plotted as a function of ΔT, as shown in Fig. 8. The τ values tend to slightly increase initially with decreasing temperature in the higher N_{TB} temperature region, immediately below the N phase. This initial increase in τ is attributable to heat fluctuations that occur close to the fluidic N phase, such that τ becomes larger. It is interesting to note that the correlation lengths and the resulting number of the helical stacks of CBCOO*n*SCB are calculated to be more than twice the corresponding values of CBOCO*n*SCB (Fig. 8). These larger correlation lengths of the helices of CBCOO*n*SCB as compared to those of CBOCO*n*SCB are reasonable, considering

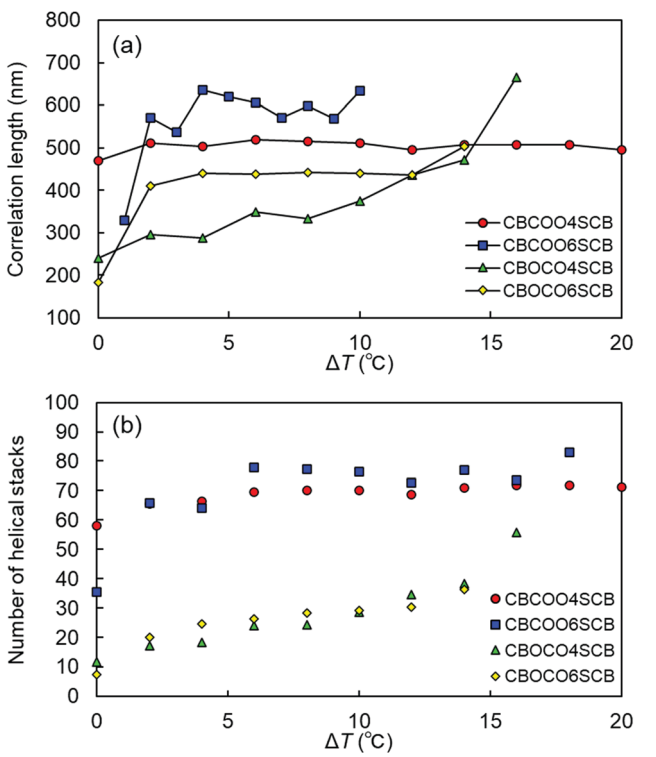

Fig. 8 (a) Correlation length (Å) and (b) helical stacks based on TReXS data scanned at 2471 eV.

their rigid molecular structures and approximately temperature-independent helical behavior, which are reminiscent of rigid packing. The helical pitches and correlation lengths of CBCOO*n*SCB are also essentially temperature-independent; and the estimated helical stacks naturally display a similar behavior. On the other hand, since the helical pitches of CBOCO*n*SCB typically depend on temperature, the helical stacks increase with decreasing temperature.

Conclusions

We herein reported the development of two homologous series of unsymmetrical ester- and thioether-linked cyanobiphenyl-based LC dimers, *viz.* CBCOO*n*SCB and CBOCO*n*SCB (n = 2, 4, 6, 8, and 10). We observed that all the dimers were mesogenic, and that CBCOO*n*SCB and CBOCO*n*SCB (n = 4, 6, 8, and 10) formed N_{TB} phases. In particular, CBCOO*n*SCB and CBOCO*n*SCB (n = 4 and 6) exhibited the N_{TB} phase across a wide temperature range. These phases were stable down to room temperature and eventually formed N_{TB} glasses. The phase-transition temperatures (excluding glass transition temperatures), and associated enthalpy and entropy changes were mostly lower for CBCOO*n*SCB than those observed for CBOCO*n*SCB. In addition, CBCOO*n*SCB and CBOCO*n*SCB (n = 4 and 6) displayed different phase-transition properties and striped optical textures. Finally, their distinct helical structures were elucidated using TReXS measurements at the sulfur K-edge. Compared with those of the typical twist-bend nematogenic dimers, CBCOO*n*SCB (n = 4 and 6) exhibited smaller pitch lengths with weaker temperature dependence, whereas CBOCO*n*SCB (n = 4 and 6) exhibited greater helical pitch lengths. The difference is ascribed to the molecular bend (or the molecular biaxiality) and structural rigidity. This study therefore provides new insights into the influence of molecular design in the N_{TB} phase, revealing that subtle structural modifications (*i.e.*, oppositely directed esters) crucially impact helical nanostructures in the N_{TB} phase.

Experimental section

The synthetic scheme and procedures and characterization data for CBCOO*n*SCB and CBOCO*n*SCB are described in the ESI.† The molecules were purified using column chromatography on silica gel and recrystallization. ^{1}H and ^{13}C nuclear magnetic resonance (NMR) spectroscopy were recorded on a JNM-ECS400 (400 MHz for ^{1}H and 100 MHz for ^{13}C) or a JNM-ECX500 (500 MHz for ^{1}H NMR and 126 MHz for ^{13}C NMR) (JEOL Ltd, Tokyo Japan). Fourier transform infrared spectroscopy (FTIR) were performed by the KBr (purchased from FUJIFILM Wako Pure Chemical Co.) method using a JASCO FT/IR-4200. High-resolution mass spectrometry (HRMS) using high-performance liquid chromatography (HPLC) (Agilent 1200 HPLC-Chip and 6520 Accurate-Mass Q-TOF) was conducted. Phase-transition behavior was studied based on POM with an Olympus (Tokyo, Japan) polarized optical microscope (BX50) with a Linkam (Surrey, UK) temperature controller LK-600PM and differential scanning calorimetry (DSC) with a Shimadzu (Kyoto, Japan) DSC 60 at a rate of 10 °C min^{-1} under a flow of nitrogen gas (50 mL min^{-1}). The POM images and DSC results for all the compounds are shown in the main text or ESI.† X-ray diffraction (XRD) measurements were conducted using a Bruker D8 DISCOVER equipped with a Vantec-500 detector using Cu-K_α radiation. The specimens, kept in capillary glass tubes of 1.5 mm diameter (purchased from WJM-Glass Müller GmbH), were aligned under a magnetic field (B = 300 mT). According to the literature,[25] TReXS measurement was performed at the beamline 5.3.1 at the Advanced Light Source, Lawrence Berkeley National Laboratory. The X-ray beam energy was tuned around the S K-edge, 2472 eV, with a channel cut double-bounce silicon (111) monochromator. A two-dimensional (2D) Pilatus detector (300 K, Dectris, Inc.) was used to collect the scattering patterns, which were subsequently converted to one-dimensional line profiles using the Nika software package.[86] The scattering patterns were viewed with the Xi-Cam interface[87] at the beamline. The sample-detector distance was tuned between 488 mm and 250 mm to access relevant q range. The beam centers and the sample-to-detector distances were calibrated using both silver behenate and 8CB.

Conflicts of interest

There are no conflicts to declare.

Acknowledgements

We are grateful to the financial supports (the Japan Society for the Promotion of Science KAKENHI grant no. 17K14493 and 20K15351, the Naito Research Grant, and research grants from the Toukai Foundation for Technology and Toyohashi University of Technology). We would like to thank Prof. Masatoshi Tokita (Tokyo Institute of Technology) for use of the instruments for XRD measurements, and Ms Tsugumi Shiokawa and Dr Hiroko Tada in the Division of Instrumental Analysis (Okayama University) for the mass measurements. We acknowledge use of Beamlines 5.3.1 of the Advanced Light Source supported by the Director of the Office of Science, Office of Basic Energy Sciences, of the U.S. Department of Energy under contract no. DE-AC02-05CH11231.

References

1 T. Sekine, T. Niori, J. Watanabe, T. Furukawa, S. W. Choi and H. Takezoe, Spontaneous helix formation in smectic liquid crystals comprisingachiral molecules, *J. Mater. Chem.*, 1997, **7**, 1307.
2 D. R. Link, G. Natale, R. F. Shao, J. E. Maclennan, N. A. Clark, E. Korblova and D. M. Walba, Spontaneous formation of macroscopic chiral domains in a fluid smectic phase of achiral molecules, *Science*, 1997, **278**, 1924.
3 G. Pelzl, A. Eremin, S. Diele, H. Kresse and W. Weissflog, Spontaneous chiral ordering in the nematic phase of an

achiral banana-shaped compound, *J. Mater. Chem.*, 2002, **12**, 2591.

4 V. Görtz and J. W. Goodby, Enantioselective segregation in achiral nematic liquid crystals, *Chem. Commun.*, 2005, 3262.

5 W. Weissflog, G. Naumann, B. Kosata, M. W. Schröder, A. Eremin, S. Diele, Z. Vakhovskaya, H. Kresse, R. Friedemann, S. A. Rama Krishnan and G. Pelzl, Ten isomeric five-ring bent-core mesogens: the influence of the direction of the carboxyl connecting groups on the mesophase behaviour, *J. Mater. Chem.*, 2005, **15**, 4328.

6 T. Kajitani, H. Masu, S. Kohmoto, M. Yamamoto, K. Yamaguchi and K. Kishikawa, Generation of a Chiral Mesophase by Achiral Molecules: Absolute Chiral Induction in the Smectic C Phase of 4-Octyloxyphenyl 4-Octyloxybenzoate, *J. Am. Chem. Soc.*, 2005, **127**(4), 1124.

7 R. Deb, R. Kanti Nath, M. Kumar Paul, N. V. S. Rao, F. Tuluri, Y. Shen, R. Shao, D. Chen, C. Zhu, I. I. Smalyukh and N. A. Clark, Four-ring achiral unsymmetrical bent core molecules forming strongly fluorescent smectic liquid crystals with spontaneous polar and chiral ordered B7 and B1 phases, *J. Mater. Chem.*, 2010, **20**, 7332.

8 H. Kim, A. Zep, S. H. Ryu, H. Ahn, T. J. Shin, S. B. Lee, D. Pociecha, E. Gorecka and D. K. Yoon, Linkage-length dependent structuring behaviour of bent-core molecules in helical nanostructures, *Soft Matter*, 2016, **12**, 3326.

9 H. Sasaki, Y. Takanishi, J. Yamamoto and A. Yoshizawa, Achiral flexible liquid crystal trimers exhibiting chiral conglomerates, *Soft Matter*, 2016, **12**, 3331.

10 A. Lehmann, M. Alaasar, M. Poppe, S. Poppe, M. Prehm, M. Nagaraj, S. P. Sreenilayam, Y. P. Panarin, J. K. Vij and C. Tschierske, Stereochemical Rules Govern the Soft Self-Assembly of Achiral Compounds: Understanding the Heliconical Liquid-Crystalline Phases of Bent-Core Mesogens, *Chem. – Eur. J.*, 2020, **26**, 4714–4733.

11 R. B. Meyer, in *Structural Problems in Liquid Crystal Physics, Molecular Fluids: Summer School in Theoretical Physics, les Houches lectures 1973*, ed. R. Balian and G. Weil, Gordon and Breach, New York, 1976, pp. 271–343.

12 I. Dozov, On the spontaneous symmetry breaking in the mesophases of achiral banana-shaped molecules, *Europhys. Lett.*, 2001, **56**, 247.

13 R. Memmer, Liquid crystal phases of achiral banana-shaped molecules: a computer simulation study, *Liq. Cryst.*, 2002, **29**, 483.

14 M. Cestari, S. Diez-Berart, D. A. Dunmur, A. Ferrarini, M. R. de La Fuente, D. J. B. Jackson, D. O. Lopez, G. R. Luckhurst, M. A. Perez-Jubindo, R. M. Richardson, J. Salud, B. A. Timimi and H. Zimmermann, Phase behavior and properties of the liquid-crystal dimer 1″,7″-bis(4-cyanobiphenyl-4′-yl) heptane: a twist-bend nematic liquid crystal, *Phys. Rev. E: Stat., Nonlinear, Soft Matter Phys.*, 2011, **84**, 031704.

15 A. G. Vanakaras and D. J. Photinos, A molecular theory of nematic–nematic phase transitions in mesogenic dimers, *Soft Matter*, 2016, **12**, 2208.

16 A. G. Vanakaras and D. J. Photinos, Molecular dynamics simulations of nematic phases formed by cyano-biphenyl dimers, *Liq. Cryst.*, 2018, **45**, 2184.

17 L. M. Heist, E. T. Samulski, C. Welch, Z. Ahmed, G. H. Mehl, A. G. Vanakaras and D. J. Photinos, Probing molecular ordering in the nematic phases of para-linked bimesogen dimers through NMR studies of flexible prochiral solutes, *Liq. Cryst.*, 2020, DOI: 10.1080/02678292.2019.1711214.

18 W. D. Stevenson, X. Zeng, C. Welch, A. K. Thakur, G. Ungar and G. H. Mehl, Macroscopic chirality of twist-bend nematic phase in bent dimers confirmed by circular dichroism, *J. Mater. Chem. C*, 2020, **8**, 1041.

19 C. Meyer, G. R. Luckhurst and I. Dozov, Flexoelectrically driven electroclinic effect in the twist-bend nematic phase of achiral molecules with bent shapes, *Phys. Rev. Lett.*, 2013, **111**, 067801.

20 D. Chen, J. H. Porada, J. B. Hooper, A. Klittnick, Y. Shen, M. R. Tuchband, E. Korblova, D. Bedrov, D. M. Walba, M. A. Glaser, J. E. Maclennan and N. A. Clark, Chiral heliconical ground state of nanoscale pitch in a nematic liquid crystal of achiral molecular dimers, *Proc. Natl. Acad. Sci. U. S. A.*, 2013, **110**, 15931.

21 V. Borshch, Y.-K. Kim, J. Xiang, M. Gao, A. Jákli, V. P. Panov, J. K. Vij, C. T. Imrie, M. G. Tamba, G. H. Mehl and O. D. Lavrentovich, Nematic twist-bend phase with nanoscale modulation of molecular orientation, *Nat. Commun.*, 2013, **4**, 2635.

22 C. Zhu, M. R. Tuchband, A. Young, M. Shuai, A. Scarbrough, D. M. Walba, J. E. Maclennan, C. Wang, A. Hexemer and N. A. Clark, Resonant Carbon K-Edge Soft X-Ray Scattering from Lattice-Free Heliconical Molecular Ordering: Soft Dilative Elasticity of the Twist-Bend Liquid Crystal Phase, *Phys. Rev. Lett.*, 2016, **116**, 147803.

23 W. D. Stevenson, Z. Ahmed, X. B. Zeng, C. Welch, G. Ungar and G. H. Mehl, Molecular organization in the twist-bend nematic phase by resonant X-ray scattering at the Se K-edge and by SAXS, WAXS and GIXRD, *Phys. Chem. Chem. Phys.*, 2017, **19**, 13449.

24 M. Salamończyk, R. J. Mandle, A. Makal, A. Liebman-Peláez, J. Feng, J. W. Goodby and C. Zhu, Double helical structure of the twist-bend nematic phase investigated by resonant X-ray scattering at the carbon and sulfur K-edges, *Soft Matter*, 2018, **14**, 9760.

25 Y. Cao, J. Feng, A. Nallapaneni, Y. Arakawa, K. Zhao, G. H. Mehl, F. Liu and C. Zhu, Identification of New Assembly Mode in the Heliconical Nematic Phase via Tender Resonant X-ray Scattering, arXiv:1907.11330.

26 E. Cruickshank, M. Salamończyk, D. Pociecha, G. J. Strachan, J. M. D. Storey, C. Wang, J. Feng, C. Zhu, E. Gorecka and C. T. Imrie, Sulfur-linked cyanobiphenyl-based liquid crystal dimers and the twist-bend nematic phase, *Liq. Cryst.*, 2019, **46**, 1595.

27 Y. Cao, C. Feng, A. Jakli, C. Zhu and F. Liu, Deciphering chiral structures in soft materials *via* resonant soft and tender X-ray scattering, *Giant*, 2020, **2**, 100018.

28 J. Xiang, Y. Li, Q. Li, D. A. Paterson, J. M. D. Storey, C. T. Imrie and O. D. Lavrentovich, Electrically Tunable Selective Reflection of Light from Ultraviolet to Visible and Infrared by Heliconical Cholesterics, *Adv. Mater.*, 2015, **27**, 3014.

29 J. Xiang, A. Varanytsia, F. Minkowski, D. A. Paterson, J. M. D. Storey, C. T. Imrie, O. D. Lavrentovich and P. Palffy-Muhoray, Electrically tunable laser based on oblique heliconical cholesteric liquid crystal, *Proc. Natl. Acad. Sci. U. S. A.*, 2016, **113**, 12925–12928.

30 Y. Wang, Z. Zheng, H. K. Bisoyi, K. G. Gutierrez-Cuevas, L. Wang, R. S. Zola and Q. Li, Thermally reversible full color selective reflection in a self-organized helical superstructure enabled by a bent-core oligomesogen exhibiting a twist-bend nematic phase, *Mater. Horiz.*, 2016, **3**, 442.

31 M. Mrukiewicz, O. S. Iadlovska, G. Babakhanova, S. Siemianowski, S. V. Shiyanovskii and O. D. Lavrentovich, Wide temperature range of an electrically tunable selective reflection of light by oblique helicoidal cholesteric, *Liq. Cryst.*, 2019, **46**, 1544.

32 S. Krishna Prasad, P. Lakshmi Madhuri, P. Satapathy and C. V. Yelamaggad, A soft-bent dimer composite exhibiting twist-bend nematic phase: photo-driven effects and an optical memory device, *Appl. Phys. Lett.*, 2018, **112**, 253701.

33 V. Sridurai, M. B. Kanakala, C. V. Yelamaggad and G. G. Nair, Effect of gelation on the Frank elastic constants in a liquid crystalline mixture exhibiting a twist bend nematic phase, *Soft Matter*, 2019, **15**, 9982.

34 S. Aya, P. Salamon, D. A. Paterson, J. M. D. Storey, C. T. Imrie, F. Araoka, A. Jákli and Á. Buka, Fast-and-giant photorheological effect in a liquid crystal dimer, *Adv. Mater. Interfaces*, 2019, **6**, 1802032.

35 C. Feng, J. Feng, R. Saha, Y. Arakawa, J. Gleeson, S. Sprunt, C. Zhu and A. Jákli, Manipulation of the nanoscale heliconical structure of a twist-bend nematic material with polarized light, *Phys. Rev. Res.*, 2020, **2**, 032004.

36 V. P. Panov, M. Nagaraj, J. K. Vij, Y. P. Panarin, A. Kohlmeier, M. G. Tamba, R. A. Lewis and G. H. Mehl, Spontaneous Periodic Deformations in Nonchiral Planar-Aligned Bimesogens with a Nematic-Nematic Transition and a Negative Elastic Constant, *Phys. Rev. Lett.*, 2010, **105**, 167801.

37 P. A. Henderson and C. T. Imrie, Methylene-linked liquid crystal dimers and the twist-bend nematic phase, *Liq. Cryst.*, 2011, **38**, 1407.

38 R. J. Mandle, E. J. Davis, S. A. Lobato, C.-C. A. Vol, S. J. Cowling and J. W. Goodby, Synthesis and characterisation of an unsymmetrical, ether-linked, fluorinated bimesogen exhibiting a new polymorphism containing the N_{TB} or 'twist-bend' phase, *Phys. Chem. Chem. Phys.*, 2014, **16**, 6907.

39 R. J. Mandle, E. J. Davis, C. T. Archbold, C. C. A. Voll, J. L. Andrews, S. J. Cowling and J. W. Goodby, Apolar bimesogens and the incidence of the twist-bend nematic phase, *Chem. – Eur. J.*, 2015, **21**, 8158.

40 R. J. Mandle and J. W. Goodby, Does Topology Dictate the Incidence of the Twist-Bend Phase? Insights Gained from Novel Unsymmetrical Bimesogens, *Chem. – Eur. J.*, 2016, **22**, 18456.

41 N. Sebastián, D. O. López, B. Robles-Hernández, M. R. de la Fuente, J. Salud, M. A. Pérez-Jubindo, D. A. Dunmur, G. R. Luckhurst and D. J. B. Jackson, Dielectric, calorimetric and mesophase properties of 1″-(2′,4-difluorobiphenyl-4′-yloxy)-9″-(4-cyanobiphenyl-4′-yloxy) nonane: an odd liquid crystal dimer with a monotropic mesophase having the characteristics of a twist-bend nematic phase, *Phys. Chem. Chem. Phys.*, 2014, **16**, 21391.

42 Z. Ahmed, C. Welch and G. H. Mehl, The design and investigation of the self-assembly of dimers with two nematic phases, *RSC Adv.*, 2015, **5**, 93513.

43 M. G. Tamba, S. M. Salili, C. Zhang, A. Jákli, G. H. Mehl, R. Stannarius and A. Eremin, A fibre forming smectic twist–bent liquid crystalline phase, *RSC Adv.*, 2015, **5**, 11207.

44 N. Sebastián, M. G. Tamba, R. Stannarius, M. R. de la Fuente, M. Salamończyk, G. Cukrov, J. Gleeson, S. Sprunt, A. Jákli, C. Welch, Z. Ahmed, G. H. Mehl and A. Eremin, Mesophase structure and behaviour in bulk and restricted geometry of a dimeric compound exhibiting a nematic–nematic transition, *Phys. Chem. Chem. Phys.*, 2016, **18**, 19299.

45 R. J. Mandle, C. T. Archbold, J. P. Sarju, J. L. Andrews and J. W. Goodby, The dependency of nematic and twist-bend mesophase formation on bend angle, *Sci. Rep.*, 2016, **6**, 36682.

46 A. A. Dawood, M. C. Grossel, G. R. Luckhurst, R. M. Richardson, B. A. Timimi, N. J. Wells and Y. Z. Yousif, On the twist-bend nematic phase formed directly from the isotropic phase, *Liq. Cryst.*, 2016, **43**, 2.

47 A. A. Dawood, M. C. Grossel, G. R. Luckhurst, R. M. Richardson, B. A. Timimi, N. J. Wells and Y. Z. Yousif, Twist-bend nematics, liquid crystal dimers, structure–property relations, *Liq. Cryst.*, 2017, **44**, 106.

48 J. P. Abberley, R. Killah, R. Walker, J. M. D. Storey, C. T. Imrie, M. Salamończyk, C. Zhu, E. Gorecka and D. Pociecha, Heliconical smectic phases formed by achiral molecules, *Nat. Commun.*, 2018, **9**, 228.

49 A. Knežević, M. Sapunar, A. Buljan, I. Dokli, Z. Hameršak, D. Kontrec and A. Lesac, Fine-tuning the effect of π–π interactions on the stability of the N_{TB} phase, *Soft Matter*, 2018, **14**, 8466.

50 K. Watanabe, T. Tamura, S. Kang and M. Tokita, Twist bend nematic liquid crystals prepared by one-step condensation of 4-(4-pentylcyclohexyl) benzoic acid and alkyl diol, *Liq. Cryst.*, 2018, **45**, 924.

51 Y. Arakawa, K. Komatsu and H. Tsuji, Twist-bend nematic liquid crystals based on thioether linkage, *New J. Chem.*, 2019, **43**, 6786.

52 Y. Arakawa and H. Tsuji, Selenium-linked liquid crystal dimers for twist-bend nematogens, *J. Mol. Liq.*, 2019, **289**, 111097.

53 Y. Arakawa, K. Komatsu, S. Inui and H. Tsuji, Thioether-linked liquid crystal dimers and trimers: the twist-bend nematic phase, *J. Mol. Struct.*, 2020, **1199**, 126913.

54 R. J. Mandle and J. W. Goodby, Molecular Flexibility and Bend in Semi-Rigid Liquid Crystals: Implications for the Heliconical Nematic Ground State, *Chem. – Eur. J.*, 2019, **25**, 14454.

55 A. Zep, K. Pruszkowska, Ł. Dobrzycki, K. Sektas, P. Szałański, P. H. Marek, M. K. Cyrański and R. R. Sicinski, Cholesterol-based photo-switchable mesogenic dimers. Strongly bent

molecules versus an intercalated structure, *CrystEngComm*, 2019, **21**, 2779.

56 Y. Arakawa, Y. Ishida and H. Tsuji, Ether- and Thioether-Linked Naphthalene-Based Liquid-Crystal Dimers: Influence of Chalcogen Linkage and Mesogenic-Arm Symmetry on the Incidence and Stability of the Twist-Bend Nematic Phase, *Chem. – Eur. J.*, 2020, **26**, 3767.

57 Y. Arakawa, K. Komatsu, Y. Ishida and H. Tsuji, Thioether-linked azobenzene-based liquid crystal dimers exhibiting the twist-bend nematic phase over a wide temperature range, *Liq. Cryst.*, 2020, DOI: 10.1080/02678292.2020.1800848.

58 R. J. Mandle and J. W. Goodby, Progression from nano to macro science in soft matter systems: dimers to trimers and oligomers in twist-bend liquid crystals, *RSC Adv.*, 2016, **6**, 34885.

59 Z. Parsouzi, G. Babakhanova, M. Rajabi, R. Saha, P. Gyawali, T. Turiv, H. Wang, A. R. Baldwin, C. Welch, G. H. Mehl, J. T. Gleeson, A. Jákli, O. D. Lavrentovich and S. Sprunt, Pretransitional behavior of viscoelastic parameters at the nematic to twist-bend nematic phase transition in flexible *n*-mers, *Phys. Chem. Chem. Phys.*, 2019, **21**, 13078.

60 A. Al-Janabi, R. J. Mandle and J. Goodby, Isomeric trimesogens exhibiting modulated nematic mesophases, *RSC Adv.*, 2017, **7**, 47235.

61 M. R. Tuchband, D. A. Paterson, M. Salamończyk, V. A. Norman, A. N. Scarbrough, E. Forsyth, E. Garcia, C. Wang, J. M. D. Storey, D. M. Walba, S. Sprunt, A. Jákli, C. Zhu, C. T. Imrie and N. A. Clark, Distinct differences in the nanoscale behaviors of the twist-bend liquid crystal phase of a flexible linear trimer and homologous dimer, *Proc. Natl. Acad. Sci. U. S. A.*, 2019, **116**, 10698.

62 R. J. Mandle and A. Al-Janabi, Utilising Saturated Hydrocarbon Isosteres of para Benzene in the Design of Twist-Bend Nematic Liquid Crystals, *ChemPhysChem*, 2020, **21**, 697.

63 Y. Arakawa, K. Komatsu and H. Tsuji, Submitted.

64 R. J. Mandle and J. W. Goodby, A Liquid Crystalline Oligomer Exhibiting Nematic and Twist-Bend Nematic Mesophases, *ChemPhysChem*, 2016, **17**, 967.

65 F. P. Simpson, R. J. Mandle, J. N. Moore and J. W. Goodby, Investigating the Cusp between the nano- and macro-sciences in supermolecular liquid-crystalline twist-bend nematogens, *J. Mater. Chem. C*, 2017, **5**, 5102.

66 Y. Wang, G. Singh, D. M. Agra-Kooijman, M. Gao, H. K. Bisoyi, C. Xue, M. R. Fisch, S. Kumar and Q. Li, Room temperature heliconical twist-bend nematic liquid crystal, *CrystEngComm*, 2015, **17**, 2778.

67 S. M. Jansze, A. Martínez-Felipe, J. M. D. Storey, A. T. M. Marcelis and C. T. Imrie, A Twist-Bend Nematic Phase Driven by Hydrogen Bonding, *Angew. Chem., Int. Ed.*, 2015, **54**, 643.

68 R. J. Mandle and J. W. Goodby, A Nanohelicoidal Nematic Liquid Crystal Formed by a Non-Linear Duplexed Hexamer, *Angew. Chem., Int. Ed.*, 2018, **57**, 7096.

69 R. Walker, D. Pociecha, A. Martinez-Felipe, J. M. D. Storey, E. Gorecka and C. T. Imrie, Twist-Bend Nematogenic Supramolecular Dimers and Trimers Formed by Hydrogen Bonding, *Crystals*, 2020, **10**, 175.

70 W. D. Stevenson, J. An, X. B. Zeng, M. Xue, H. X. Zou, Y. S. Liu and G. Ungar, Twist-bend nematic phase in biphenylethane-based copolyethers, *Soft Matter*, 2018, **14**, 3003.

71 D. Chen, M. Nakata, R. Shao, M. R. Tuchband, M. Shuai, U. Baumeister, W. Weissflog, D. M. Walba, M. A. Glaser, J. E. Maclennan and N. A. Clark, Twist-bend heliconical chiral nematic liquid crystal phase of an achiral rigid bent-core mesogen, *Phys. Rev. E: Stat., Nonlinear, Soft Matter Phys.*, 2014, **89**, 022506.

72 P. Sreenilayam, V. P. Panov, J. K. Vij and G. Shanker, The N_{TB} phase in an achiral asymmetrical bent-core liquid crystal terminated with symmetric alkyl chains, *Liq. Cryst.*, 2017, **44**, 244.

73 J. W. Emsley, G. R. Luckhurst, G. N. Shilstone and I. Sage, The preparation and properties of the α,ω-bis (4,4′-cyanobiphenyloxy) alkanes: nematogenic molecules with a flexible core, *Mol. Cryst. Liq. Cryst.*, 1984, **102**, 223.

74 P. K. Challa, V. Borshch, O. Parri, C. T. Imrie, S. N. Sprunt, J. T. Gleeson, O. D. Lavrentovich and A. Jákli, Twist-bend nematic liquid crystals in high magnetic fields, *Phys. Rev. E: Stat., Nonlinear, Soft Matter Phys.*, 2014, **89**, 060501(R).

75 J. Zhou, W. Tang, Y. Arakawa, H. Tsuji and S. Aya, Viscoelastic properties of a thioether-based heliconical twist-bend nematogen, *Phys. Chem. Chem. Phys.*, 2020, **22**, 9593.

76 W. D. Stevenson, H. X. Zou, X. B. Zeng, C. Welch, G. Ungar and G. H. Mehl, Dynamic calorimetry and XRD studies of the nematic and twist-bend nematic phase transitions in a series of dimers with increasing spacer length, *Phys. Chem. Chem. Phys.*, 2018, **20**, 25268.

77 C. Meyer, G. R. Luckhurst and I. Dozov, The temperature dependence of the heliconical tilt angle in the twist-bend nematic phase of the odd dimer CB7CB, *J. Mater. Chem. C*, 2015, **3**, 318.

78 G. Singh, J. Fu, D. M. Agra-Kooijman, J.-K. Song, M. R. Vengatesan, M. Srinivasarao, M. R. Fisch and S. Kumar, X-ray and Raman scattering study of orientational order in nematic and heliconical nematic liquid crystals, *Phys. Rev. E*, 2016, **94**, 060701(R).

79 D. M. Agra-Kooijman, G. Singh, M. R. Fisch, M. R. Vengatesan, J.-K. Song and S. Kumar, The oblique chiral nematic phase in calamitic bimesogens, *Liq. Cryst.*, 2017, **44**, 191.

80 R. J. Mandle and J. W. Goodby, Order parameters, orientational distribution functions and heliconical tilt angles of oligomeric liquid crystals, *Phys. Chem. Chem. Phys.*, 2019, **21**, 6839.

81 K. Merkel, A. Kocot, C. Welch and G. H. Mehl, Soft modes of the dielectric response in the twist-bend nematic phase and identification of the transition to a nematic splay bend phase in the CBC7CB dimer, *Phys. Chem. Chem. Phys.*, 2019, **21**, 22839.

82 J. F. Yan, G. Vanderkooi and H. A. Scheraga, Conformational Analysis of Macromolecules. V. Helical Structures of Poly-L-aspartic Acid and Poly-L-glutamic Acid, and Related Compounds, *J. Chem. Phys.*, 1968, **49**, 2713.

83 M. Perricaudet and A. Pullman, An *ab initio* quantum-mechanical investigation on the rotational isomerism in amides and esters, *Int. J. Pept. Protein Res.*, 1973, **5**, 99.
84 M. Cotrait, P. Marsau, M. Pesquer and V. Volpilhac, Molecular arrangement of mesogenic disc-like compounds: the hexa-*n*-alkoxy and hexa-*n*-alkanoyloxy triphenylenes, *J. Physiol.*, 1982, **43**, 355.
85 S. Ananda Rama Krishnan, W. Weissflog, G. Pelzl, S. Diele, H. Kresse, Z. Vakhovskaya and R. Friedemann, DFT and MD studies on the influence of the orientation of ester linkage groups in banana-shaped mesogens, *Phys. Chem. Chem. Phys.*, 2006, **8**, 1170.
86 J. Ilavsky, Nika: software for two-dimensional data reduction. Nika: software for two-dimensional data reduction, *J. Appl. Crystallogr.*, 2012, **45**, 324.
87 R. J. Pandolfi, *et al.*, Xi-cam: a versatile interface for data visualization and analysis, *J. Synchrotron Radiat.*, 2018, **25**, 1261.